

PAPER • OPEN ACCESS

## Bandwidth enhancement in Hall probe by X-Hall DC biasing

To cite this article: M Crescentini *et al* 2018 *J. Phys.: Conf. Ser.* **1065** 052031

View the [article online](#) for updates and enhancements.



**IOP | ebooks™**

Bringing you innovative digital publishing with leading voices to create your essential collection of books in STEM research.

Start exploring the [collection](#) - download the first chapter of every title for free.

## Bandwidth enhancement in Hall probe by X-Hall DC biasing

M Crescentini<sup>1,2</sup>, M Biondi<sup>2</sup>, M. Marchesi<sup>3</sup>, A. Romani<sup>1,2</sup>, M Tartagni<sup>1,2</sup>,  
and P A Traverso<sup>1</sup>

<sup>1</sup>DEI, University of Bologna, Viale del Risorgimento, Bologna, Italy

<sup>2</sup>ARCES, University of Bologna, Via Venezia 52, Cesena, Italy

<sup>3</sup>Analog and Smart Power Technology, STMicroelectronics, Castelletto (MI), Italy

m.crescentini@unibo.it

**Abstract.** The spinning-current technique is the state-of-the-art method for offset cancellation in Hall-effect probe. This technique achieves the best results in terms of offset reduction but limits the acquisition bandwidth to less than 1 MHz; therefore, it precludes the use of purely Hall-effect sensors in broadband current measurement. We present the X-Hall probe, a DC bias approach combined with an octagonal 8-contact morphology of the Hall-effect probe, which overcomes the bandwidth limitations of spinning-current-operated Hall sensors while reducing the offset. A prototype of the X-Hall probe is realized in CMOS-like technology and can potentially achieve a bandwidth wider than 40 MHz with an acceptable residual offset.

### 1. Introduction

The operating frequencies typical of power circuits used in electric vehicles are nowadays increasing to allow the shrinking of the passive components [1]. In this context, the development of CMOS-compatible, isolated and broadband (> 1 MHz) current sensors is of main interest, since it will allow the design of integrated *smart-power* circuits, i.e. power circuits with sensing and logic features integrated into the same silicon chip.

The most common solution for isolated current sensing, which is also compatible with CMOS technology, is based on a solid-state Hall-effect probe biased by implementing the spinning-current technique, which is devoted to the compensation of the offset. This technique consists in a periodical rotation of the bias current by 90 degrees at a frequency  $f_{spin}$  that, due to reciprocity relationship of the Hall-effect probe, modulates the intrinsic offset at  $f_{spin}/2$  while the signal remains in the baseband. Therefore, a simple averaging over a full rotation cycle nominally eliminates the modulated offset. This technique demonstrated to be the best offset-compensation method, so far, but commercial sensors implementing this solution are limited in bandwidth to a few hundred kilohertz.

The main bandwidth limits in Hall-effect probe are (ordered by decreasing cut-off frequency): *i*) a *physical* limit, due to relaxation time of the charge carriers [2]; *ii*) a *fundamental* limit (*technological* in the following), set by the intrinsic equivalent capacitance of the probe itself; *iii*) a more *practical* limit (*electronic* in the following), set by the input capacitance of the embedding circuits, which increases the total capacitive load seen by the probe [3,4]; *iv*) a *methodological* limit, set by the need of the spinning-current technique, which limits the maximum sampling frequency and thus the acquisition bandwidth [5]. The technological limit can be treated as the maximum achievable bandwidth by the probe in case it is connected to ideal biasing and readout circuits. Real electronic circuits add their own input capacitances to the intrinsic capacitance of the probe; thus setting the electronic limit [3]. Unfortunately, operating the spinning-current technique at high  $f_{spin}$  causes an abrupt degradation of the effectiveness in offset compensation [5]. For instance, in [5] we proposed to integrate the Hall-effect probe with a novel readout circuit with minimum input capacitance on the same CMOS substrate. In this way, a 600-kHz bandwidth was demonstrated with  $f_{spin} = 8$  MHz higher than never before, but the sensor could operate at even higher  $f_{spin}$  and achieve an acquisition bandwidth wider than 1 MHz at the cost of a residual offset 100-times higher. Table I reports the bandwidth limit described above, with numerical values evaluated for a 30- $\mu\text{m}$  x 30- $\mu\text{m}$  square Hall-effect probe and the electronic system proposed in [5].



Table 1 Bandwidth limits in spinning-current operated Hall-effect probes

Bandwidth limit	Value estimated in [3,5]
Physical	1 GHz and above
Technological	~ 30 to 50 MHz
Electronic	15 MHz (with 1 pF input capacitance of the embedded electronic)
Methodological	600 kHz (before causing abrupt degradation of the offset)

In this paper, we propose a purely-DC bias strategy (with no need for spinning) which is allowed by a novel morphological design of the Hall probe and provides an adequate and bandwidth-independent reduction of the offset voltage so as to push the bandwidth towards the technological limit. Moreover, switches used for the bias rotation, timing signals, and multiple acquisition channels are no longer required, leading to a strong simplification of the electronic design. In the following, Section II describes the morphology of the probe and the novel operative configuration, while Section III presents preliminary results.

## 2. Octagonal X-Hall probe with purely-DC bias strategy

We propose an octagonal n-well as the magnetic-sensitive active region (fig. 1-a), shared by two elementary Hall-effect probes: one placed below the horizontal axis of symmetry (probe A) and one placed above (probe B). The active region is accessed through 4 wide bias contacts and 4 smaller sensing contacts. The two bias contacts L and R are shared by the two Hall-effect probes and connected to ground. The bias currents  $I_A$  and  $I_B$  (nominally identical in the final configuration) are fed through bias contacts B and T, respectively. The output voltages of the two elementary probes,  $V_A$  and  $V_B$ , are read across the sensing contacts as shown in fig. 1-a.

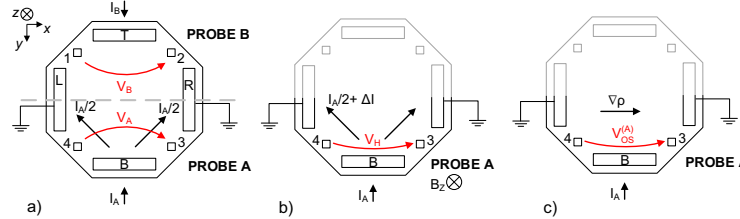


Fig. 1 a) Schematic of the octagonal Hall-effect probe. b) Unbalance of the bias current when a magnetic field is applied orthogonally to the probe. c) Generation of an offset voltage due to (e.g.) a resistivity gradient.

For the sake of better understanding, let's consider all the sensing pads as being electrically floating. If probe A is fully symmetric and homogeneous, then the current density field lines along which  $I_A$  flows are perfectly balanced with respect to the  $y$ -axis, and the voltage  $V_A$  is null. When a magnetic field component  $B_z$  is applied on the  $z$ -axis (fig. 1-b), then the current field lines become unbalanced due to the Hall effect and  $V_A = V_H$ . In case of semiconductor inhomogeneities, such as a gradient of the silicon resistivity  $\rho$  along the  $x$ -axis, an offset voltage  $V_{OS}^{(A)}$  arises independently of the presence of the magnetic field (fig. 1-c), and sums to the Hall voltage  $V_H$  so that the floating voltage  $V_A$  becomes:

$$V_A = V_H + V_{OS}^{(A)} \quad (1)$$

If the source of offset, in this case the resistivity gradient, acts in the same way on the probe B, then it gives rise to an offset voltage  $V_{OS}^{(B)}$  with the same sign as in eq. (1) and the same magnitude, if the gradient is constant throughout the probe. On the contrary, the bias current  $I_B$  has opposite direction with respect to current  $I_A$ , therefore the Hall voltage has negative sign. As a result, the voltage  $V_B$  can be written as:

$$V_B = -V_H + V_{OS}^{(B)} \quad (2)$$

By calculating the difference between the two floating voltages, we nominally cancel the offset voltage:

$$V_A - V_B = 2V_H \quad (3)$$

Equation (3) is exact if the sources of offset act similarly on both the elementary probes, but local sources of offset exist and lead to a residual offset voltage. For instance, a punctual defect of the silicon crystal is a local source of offset. Similarly, also mismatches of the bias currents unbalance the offsets. Taking into account these effects, we can rewrite eq. (3) as:

$$V_A - V_B = 2V_H + \Delta V_{OS} \quad (4)$$

where  $\Delta V_{OS}$  is the residual offset. It is worth noticing that also the residual offset voltage in spinning-current operated Hall probes is related to local sources of offset.

The probe proposed so far would require a complex readout circuit to implement (4), with rather high input capacitance that would seriously degrade the electronic limit. To simplify the overall sensor architecture and minimize the total capacitance seen by the probe while preserving the proposed approach, we short-circuit the sensing contacts along the diagonal axes as shown in fig. 2-a. The short circuits force the equality  $V_{OUT} = V_B = -V_A$  so that the Hall voltage contributions in eq. (1) and (2) can be correctly sensed at the output node. As far as the offset is concerned, the short circuits represent an additional boundary condition applied to the net charge distribution throughout the probe that forces the minimization of the magnitude of the offset contributions to  $V_B$  and  $V_A$ . More precisely, if the physical origin and sign of the offset are rigorously the same for both the elementary probes, as in the example of a constant resistivity gradient, then the only value of offset that satisfies both the symmetry of the overall probe and the boundary condition imposed by the short circuits is zero. However, a residual offset  $\Delta V'_{OS}$  in  $V_{OUT}$  is expected due to uncorrelated local defects and/or asymmetries. The amount of this residual offset will be experimentally evaluated in the next section. The final structure, as shown in fig. 2-a, requires a simple DC bias and a single differential amplifier, with no switching operations, and allows to benefit from both the absence of the methodological limit and the minimization of the overall capacitance. We name this structure X-Hall probe.

### 3. Results

A prototype of the octagonal probe was realized in STMicroelectronics BCD (Bipolar-CMOS-DMOS) technology (fig. 2-b), a 160-nm silicon technology devoted to smart-power designs that perfectly fits the application requirements. All the 8 contacts of the probe are accessible from out of the chip, so that either the X-Hall DC biasing or the spinning-current technique can be implemented. A copper strip is placed on top of the Hall probe (fig. 2-c). By driving a DC current into the copper strip, we generate a known average magnetic field  $B_z$ . The current-to-vertical-magnetic-field transduction is 1.9 mT/A, as derived in [5]. The chip is mounted on a plastic spring socket for high flexibility.

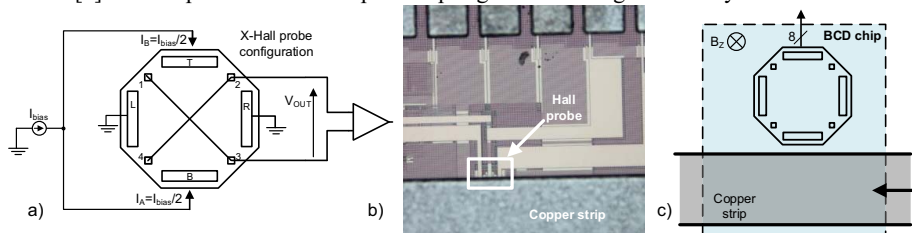


Fig. 2 a) Schematic diagram of the X-Hall probe. b) Microphotograph of the BCD prototype. c) Block diagram of the BCD prototype.

We performed a static characterization in the 2-A range to assess the correct linear behavior of the X-Hall probe. The current range corresponds to a vertical magnetic field within  $\pm 3.9$  mT. The X-Hall probe was biased with  $I_A = I_B = I_{bias}/2 = 500$   $\mu$ A. Fig. 3-a shows the corresponding measured  $V_{OUT}$  for a single sample. Non-perfect contacts in the spring socket limit the measurement uncertainty to approximately 20  $\mu$ V [6]. The X-Hall probe shows a linear response with a root mean square deviation from the linear best-fit of 1% over the full-scale (FS) range. The linear best fit leads to an estimated current-related sensitivity,  $\hat{S}_I = 165$  VA<sup>-1</sup>T<sup>-1</sup>, comparable to sensitivities of standard Hall-effect probe realized in CMOS technology [7].

To evaluate the offset-reduction effectiveness of the X-Hall probe, we operated the same octagonal probe in three different polarization arrangements: a) X-Hall configuration, b) spinning-current technique performed at low  $f_{spins}$ , c) DC bias of the octagonal probe along a diagonal direction. We replicated the measurement over 20 samples at the room temperature of 26(1) °C to perform statistical analysis. Fig. 3-b shows histograms of the occurrences of the residual offset and the estimated gaussian probability density functions (pdfs), while Table-II provides mean and standard deviation values. The X-Hall shows a reduction of the mean residual offset by a factor greater than 60 with respect to the bare sensor biased in DC mode (arrangement c). Moreover, the mean residual offset achieved by the X-Hall configuration is comparable to the residual offset resulting from the spinning-current technique; therefore, the X-Hall configuration proves to be an effective offset reduction technique.

The mean residual offset  $\overline{\Delta V'_{OS}} = -0.27$  mV achieved by the X-Hall probe is about one order of magnitude higher than the typical residual offset (tens of  $\mu$ V) achieved by state-of-the-art Hall-effect probes operated at low  $f_{spin}$  [5]. However, differently from spinning-biased probes, the residual offset in

X-Hall configuration is independent of the process of maximizing the bandwidth; thus, the acquisition bandwidth can be enlarged up to the electronic limit, without causing offset degradation. In addition, the latter limit is further moved closer to the technological one thanks to the minimization of load capacitances. Summarizing, the X-Hall probe is expected to show the lowest offset when the sensor is used in broadband (>1 MHz) applications.

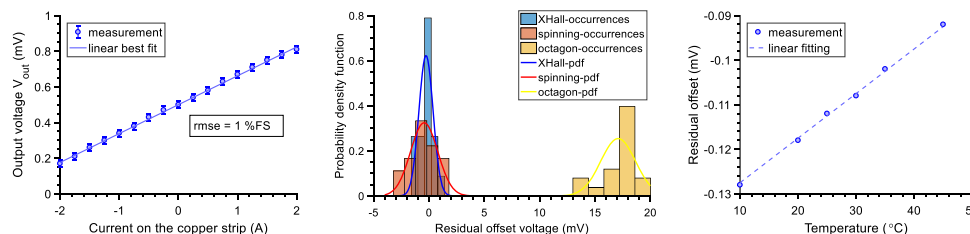


Fig. 3 a) Static characteristic of a single realization of the X-Hall probe. b) Estimated PDFs of the residual offset for different biasing strategies of the octagonal probe. c) Temperature instability of the offset in the X-Hall probe.

Table 2 Statistical parameters of residual offset

sensor configuration	mean value (mV)	standard deviation (mV)
X-Hall	-0.27	0.64
spinning-current	-0.4	1.2
octagon	17.1	1.6

The temperature-stability of the residual offset is more important than the offset value itself since it directly implies the effectiveness of calibration processes. Fig. 3-c reports a preliminary characterization of the temperature dispersion of the residual offset  $\Delta V_{os}$  measured over a 40-°C temperature range. The measurement was performed on a single sample arranged in the X-Hall scheme. The residual offset drifts in temperature with a rate of 1  $\mu\text{V}/^\circ\text{C}$ .

The test-bench for dynamic performance evaluation is not yet available since the BCD samples that have been redesigned with integrated electronic front-end to minimize the parasitic capacitance and achieve the maximum bandwidth are waiting the next scheduled foundry run. Therefore, we estimated the bandwidth by means of numerical TCAD simulations and theoretical analysis. In a recent paper, we have demonstrated that the response of the Hall-effect probe to a magnetic stimulus follows a classic first-order behavior with a time constant  $\tau$  set by the product of the equivalent resistance of the probe  $R$  and the sum of all the parasitic capacitances facing to the output node of the probe [3,8]. TCAD simulations for the X-Hall probe report  $R=3.6\text{ k}\Omega$  and an intrinsic capacitance of a few hundreds of femtofarads. On the basis of the analysis of the BCD technology and of the typical design of readout circuits, we estimated an input capacitance of the electronic circuit of approximately 600-to-800 fF. Thus, we expect an acquisition bandwidth higher than 40 MHz, in agreement with TCAD simulation. This would be the widest bandwidth ever reported by an Hall-effect probe, more than 10 times wider than the state of the art.

Summarizing, the X-Hall configuration allows exploiting the wideband capability of the Hall-effect probe up to the limit set by the electronic interface while ensuring a reduction of the intrinsic offset and keeping it constant over the full acquisition bandwidth. By using the X-Hall configuration, it would be possible to monitor very high-frequency (> 1 MHz) currents with a reduced residual offset.

## Acknowledgments

This work was funded from the ECSEL Joint Undertaking (JU) under grant agreement No 737434.

## References

- [1] Ripka P 2010 Electric current sensors: a review *Meas. Sci. Technol.* **21** 112001
- [2] Popovic R S 2004 *Hall Effect Devices* (Boca Raton (FL): CRC Press)
- [3] Crescentini M, Marchesi M, Romani A, Tartagni M and Traverso P A 2017 Bandwidth Limits in Hall Effect-based Current Sensors *Acta-IMEKO* **6** 17–24
- [4] Crescentini M, Romani A and Sangiorgi E 2014 Physical simulations of response time in Hall sensor devices *Proc. 2014 Int. Conf. on Ultimate Integration on Silicon (ULIS)* (Stockholm, Sweden: IEEE) pp 89–92
- [5] Crescentini M, Marchesi M, Romani A, Tartagni M and Traverso P A 2018 A Broadband, On-Chip Sensor Based on Hall Effect for Current Measurements in Smart Power Circuits *IEEE Trans. Instrum. Meas.* **67** 1470–85
- [6] Joint Committee for Guides in Metrology 2008 *Guide to the expression of uncertainty in measurement* (Geneva)
- [7] Crescentini M, Biondi M, Romani A, Tartagni M and Sangiorgi E 2017 Optimum Design Rules for CMOS Hall Sensors *Sensors* **17** 765
- [8] Crescentini M, et al. 2016 Experimental characterization of bandwidth limits in hall sensors *21st IMEKO TC-4 Int. Symposium* (Budapest, Hungary) pp 1–6